RARE EARTH MERCAPTOACETATE CORROSION INHIBITORS FOR AA2024-T3

R. Catubig[1,2], I. Cole[2], A. Hughes[2], B. Hinton[1] and M. Forsyth[1]*

[1]Institute of Frontier Materials, Deakin University, Burwood Victoria,
[2]Materials Science and Engineering, CSIRO, Clayton, Victoria

SUMMARY: The corrosion inhibition of the aluminium alloy AA2024 using rare earth mercaptoacetate inhibitors was investigated to elucidate the mechanisms of protection. The strong susceptibility towards localised corrosion by AA2024 has in the past been mitigated through the use of chromate-based inhibitors, however their toxic and carcinogenic nature has meant a reduction of use in all applications, including aerospace applications. Rare earth-organic compounds have shown promising successes in limiting the corrosion on AA2024, but the process of inhibition is currently not well understood. It was hypothesised that the incorporation of a thiol-containing organic into the inhibitor could lead to deposition of the inhibitor, through the sulfur, at Cu-rich sites in the AA2024 surface and effectively limit corrosion. This has led to the exploration of corrosion protection with rare earth mercaptoacetate compounds. In the current work, electrochemical testing and surface characterization techniques were utilised to examine the behaviour of rare earth mercaptoacetate inhibitors in 0.1 M sodium chloride solution. The praseodymium mercaptoacetate compound was found to reduce the average corrosion current density to a greater extent than that of the cerium mercaptoacetate compound in neutral pH conditions. The differences between the two inhibitors will be discussed.

Keywords: AA2024-T3, cerium, praseodymium, mercaptoacetate

1. INTRODUCTION

AA2024-T3 is a commonly used aerospace alloy which has a relatively high susceptibility towards localised attack due to its heterogeneous microstructure.[1] Cu-rich intermetallic (IM) particles have been shown to greatly influence the site of attack on the AA2024-T3 surface.[2] In particular, the S-phase (Al_2CuMg) particles, once dealloyed, can act as efficient cathodes and preferentially attack the adjacent matrix.[3, 4]

The use of corrosion inhibitors on alloy surfaces is an effective and cost effective strategy in controlling corrosion on these alloys. The findings of Hinton et al.[5] of the effective corrosion inhibition on AA7075 with $CeCl_3$ salts have led to a number of rare earth (RE) inhibitors to emerge which have been shown to be potential candidates to replace the efficient but toxic chromate-based inhibitors.[6, 7] Markley et al. demonstrated the ability of cerium diphenylphosphate ($Ce(dpp)_3$) to limit corrosion on AA2024-T3 in solution and as a pigment in an epoxy coating.[8] Significant reductions in the corrosion rate of AA2024-T3 over 1, 3 and 6 week immersion periods was observed by Ho et al. with the cerium dibutylphosphate ($Ce(dbp)_3$) inhibitor.[9] Due to the strong affinity of sulfur towards copper[10] and the relatively high inhibition efficiency of sodium mercaptoacetate (Na-MAcet) on AA2024-T3 as reported by Harvey,[11] it was hypothesised that a RE inhibitor complex incorporating sulfur by means of mercaptoacetate (MAcet) will result in a more effective mode of corrosion inhibition for the AA2024-T3 alloy. In the current work, cerium mercaptoacetate ($Ce(MAcet)_3$) and praseodymium mercaptoacetate ($Pr(MAcet)_3$) were synthesised to observe the effect on corrosion reactions as well as characterise the film formed by each inhibitor after 30 minutes of immersion.

2. EXPERIMENTAL DETAILS

2.1. Materials, synthesis of RE(MAcet)₃ inhibitors and test solutions

AA2024-T3 alloy samples were taken from a 2.5 mm thick sheet. Inductively Coupled Plasma Optical Emission Spectroscopy (ICP-OES) detected copper and magnesium contents of 4.63 wt% and 1.39 wt% respectively in the alloy. The RE- mercaptoacetate (RE(MAcet)₃) inhibitors were synthesised by aqueous metathesis in a solution of 50 % deionised water and 50 % analytical grade methanol. Cerium chloride ($CeCl_3 \cdot 7H_2O$, 98 wt%) or praseodymium chloride ($PrCl_3 \cdot 6H_2O$, 99.9 wt%) was mixed with sodium mercaptoacetate (Na-MAcet) (97 wt%). The molar ratio of RE with Na-MAcet prior to mixing was 1:3. After stirring at room temperature for at least 1 hour, the precipitate was filtered out and allowed to dry. The necessary amount of each inhibitor was dissolved into a solution for testing.

All inhibitors were dissolved with analytical grade 0.1 M sodium chloride (NaCl) in deionised water. The concentration of the Ce(MAcet)₃ and Pr(MAcet)₃ inhibitors when dissolved into solution was 10^{-4} M. All solutions were adjusted to pH 6 with NaOH or HCl when necessary prior to testing.

2.1. Potentiodynamic Polarisation

10 mm x 10 mm coupons were cut from the sheet of AA2024-T3 and mounted into epoxy. The specimens were ground using SiC paper with a final polishing using 1 μm alumina powder with analytical grade ethanol as the lubricant. Sonication in ethanol was performed between the final three grades of polishing and nitrogen gas was used for drying. Each sample was left in a desiccator for an hour prior to testing. A titanium mesh (approximately 700 mm² in area), saturated calomel electrode and the epoxy mounted polished AA2024-T3 specimens acted as the counter, reference and working electrodes respectively to complete the standard three electrode cell. Triplicate polarisation scans were performed after a 30 minute open circuit potential (OCP) period with a potential range of -0.3 V to 0.5 V. The scan rate was 0.1667 mV/s and the volume of each solution was 400 ml.

2.2. Immersion corrosion experiments

10 mm x 10 mm epoxy mounted AA2024-T3 coupons were prepared in the same procedure as in the polarisation experiments (section 2.1). Solutions of 50 ml in volume were prepared in separate glass containers to hold a single epoxy mounted sample for the duration of the test. The jars were left open to air and the different solutions were topped up when needed. At the conclusion of the test period, the samples were rinsed with deionised water and dried with nitrogen gas. The coupons were then removed from the epoxy to allow for analysis with the scanning electron microscope (SEM) and the energy dispersive X-ray spectroscopy (EDXS). An accelerating voltage of 10 kV was used for all samples.

3. RESULTS

3.1 Potentiodynamic polarisation

The polarisation curves for solutions immersed with no inhibitor, with 10^{-4} M Ce(MAcet)₃ and 10^{-4} M Pr(MAcet)₃ are shown in Figure 1. Correlating to previous studies, both the RE(MAcet)₃ inhibitors reduced anodic current densities to more negative potentials which is evidence of anodic inhibition. In terms of the cathodic arm, the Ce(MAcet)₃ inhibitor shifted the cathodic currents by a relatively small margin (approximately 6.4×10^{-4} mA/cm² at -0.7 V). In contrast, the Pr(MAcet)₃ inhibitor was able to shift the cathodic arm by almost 2 orders of magnitude towards more negative current densities as well as shifting the corrosion potential (E_{corr}) approximately 60 mV more negative. In addition, the Pr(MAcet)₃ inhibitor shifted E_{corr} by about 50 mV to more negative potentials. The Ce(MAcet)₃ inhibitor did not shift E_{corr} significantly compared to the control.
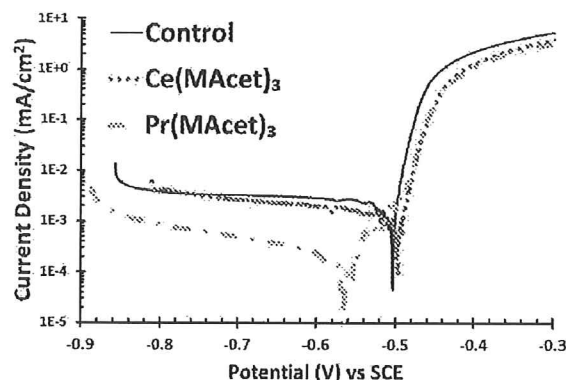
Figure 1: Potentiodynamic polarisation curves for the control (black solid line), Ce(MAcet)₃ (red dotted line) and the Pr(MAcet)₃ (green dashed line) inhibitor.

The average i_{corr} values for each solution are presented in Figure 2. Assuming that the i_{corr} was an approximation of the corrosion rate of the AA2024-T3 as the working electrode, the largest reduction in the rate of corrosion was achieved when 10^{-4} M of Pr(MAcet)₃ was added to the test solution. The Ce(MAcet)₃ inhibitor also lowered the corrosion rate relative to the control but it is clearly not as effective in protecting the AA2024-T3 surface as the Pr(MAcet)₃ inhibitor.
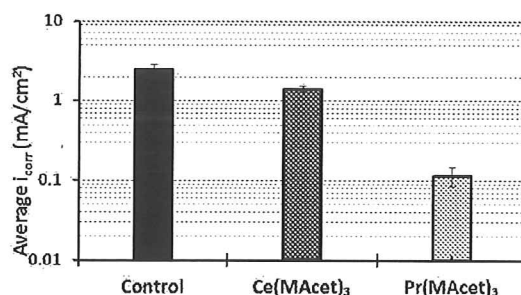

Figure 2: Average i_{corr} values for the control, Ce(MAcet)₃ and Pr(MAcet)₃ inhibitors

3.2   SEM/EDXS analysis

Secondary electron images and the corresponding EDXS maps for oxygen (d, e and f), RE metal (g and h) and sulfur (i and j) are shown in Figure 3. When no inhibitor was present (control), the majority of attack was on AlCuMg IM particles as well as dissolving the AA2024-T3 matrix immediately adjacent AA2024-T3 matrix (trenching). These are assumed to be the S-phase. Some S-phase particles showed rings or halos of what appeared to be corrosion product, the halo front can be seen on the secondary electron image of the control (Figure 3a) at site A. Other IM particles, such as the AlCuFeMnSi particle at site B showed no noticeable trenching or attack on the particles themselves. From the EDXS maps, the level of formation of oxygen-containing corrosion product on IM particles was similar to the matrix. Also, it was too difficult to distinguish the corrosion halo from the general matrix in the oxygen map (Figure 3d).

With the addition of the Ce(MAcet)₃ inhibitor, the corrosion halos were not observed around any particle. However, deposits on and around S-phase particles was found, an example is shown at site C Figure 3b. In addition to the deposits, the scratch marks from the polishing process became less visible which indicates the presence of a thin film. Similar to the control, localised attack was observed around S-phase particles and not around the periphery of other IM particles. Oxygen was detected at greater concentrations over S-phase particles with evidence of trenching (as shown in Figure 3e). Spot analysis detected cerium over all analysed S-phase particles while only a small number of other IM particles, such as AlCuFeMnSi, showed the presence of cerium. Similarly, sulfur was also only detected over S-phase particles in the spot analysis but not always at the same sites as cerium. Figure 4 shows the EDXS spectra which are typical over an S-phase particle and the alloy

matrix. Sulfur is clearly present over the S-phase but no sulfur peak was observed for the spectra over the matrix. When comparing the cerium and sulfur maps (Figure 3g and i respectively), a relatively higher concentration of cerium and sulfur was observed on the S-phase particle at site C, while the AlCuFeMnSi particle at site D illustrated the concentrated deposition of only cerium and not sulfur. The detection of cerium and sulfur over the alloy matrix in the EDXS maps of Figure 3 is likely to be from the background signal of the EDXS spectrum since spot analysis did not detect any cerium or sulfur over the matrix.
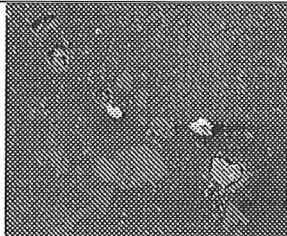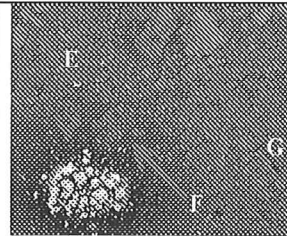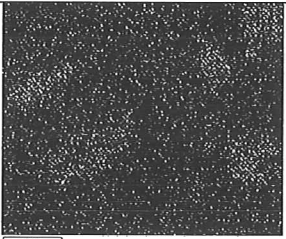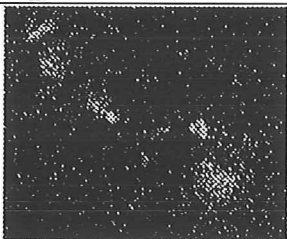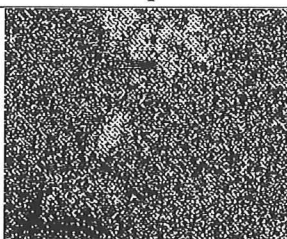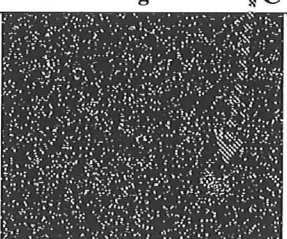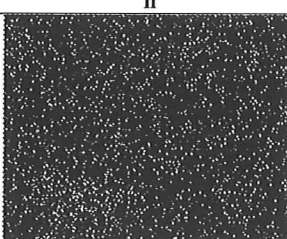
10 µm ←→	Control (NaCl)	$Ce(MAcet)_3 \ 10^{-4} M$	$Pr(MAcet)_3 \ 10^{-4} M$
5000x Secondary electron image	a	b	c
Oxygen Map	d	e	f
RE map (Ce/Pr)	N/A	g	h
Sulfur map	N/A	i	j

Figure 3: Secondary electron images and EDXS maps for the (from left) – control, $Ce(MAcet)_3$ and $Pr(MAcet)_3$ samples. (From top) The oxygen, REM and sulfur maps are also presented.

The effect of the $Pr(MAcet)_3$ inhibitor addition on the AA2024-T3 surface was very similar to the $Ce(MAcet)_3$ inhibitor. The spot analysis revealed preferential deposition of sulfur on the S-phase particle at site E (shown in Figure 3c). Praseodymium was observed at site E and the AlCuFeMn IM particle at site F but was not detected on the AlCuFeMnSi IM particle at site G. The EDXS maps detected oxygen at high concentration at site E (Figure 3f) while praseodymium was concentrated over portions of the IM particles at sites E, F and G (Figure 3h). Similar to the $Ce(MAcet)_3$ sample, the sulfur map for the $Pr(MAcet)_3$ sample (Figure 3j) detected sulfur over the whole map. The background signal from the spectra was likely to be responsible for giving false readings. The spot analysis detected Pr and S only over S-phase and not on the alloy matrix. Never-the-less, a deposited film is likely to be present over the whole surface for both $RE(MAcet)_3$ samples immersed for 30

minutes. Difficulties in the detection of RE-organic species on the alloy matrix surfaces was typical of previously studied systems such as Ce(dbp)₃.[9] In addition, the polishing scratch marks were also less visible compared to the control. A lower number of S-phase particles showed evidence of localised attack around its periphery when Pr(MAcet)₃ was added compared to Ce(MAcet)₃. The appearance of the Pr(MAcet)₃ deposits were larger and covered a larger portion of the IM particle compared to the Ce(MAcet)₃. Clearly the Pr(MAcet)₃ was limiting a number of corrosion processes that led to trenching around some S-phase particles and was more effective overall as an inhibitor relative to Ce(MAcet)₃.

A)

B)
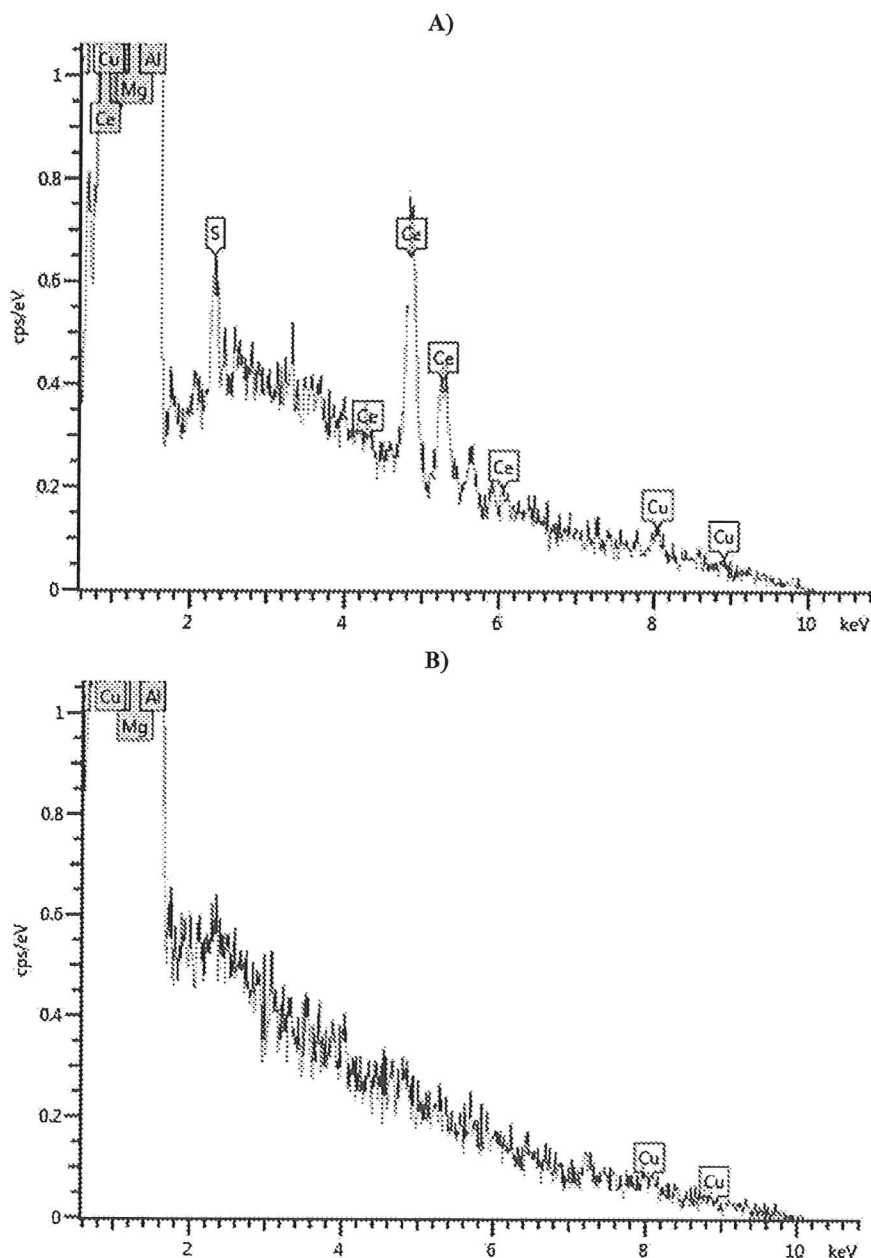

Figure 4: Typical EDXS spectra on the sample immersed with Ce(MAcet)₃ over A) S-phase particles with Ce and S B) the AA2024-T3 matrix with no Ce or S.

4. DISCUSSION

4.1. Effect of the RE(MAcet)₃ inhibitors on halo and trench formation

The lack of trenching around some S-phase particles in the presence of Pr(MAcet)₃ as well as the lack of corrosion halos around any IM particles in the presence of either of the RE(MAcet)₃ inhibitors suggest that several corrosion processes were affected by the RE(MAcet)₃ inhibitors. Corrosion halos around IM particles (as shown in Figure 3a) was previously observed by Hughes et al. within corrosion rings.[12] It was proposed by Hughes et al. that the formation of corrosion rings on AA2024-T3 immersed in a 0.1 M NaCl solution for various immersion times was due to the presence of different local conditions on other side of the ring boundary. Hughes suggested a number of possible mechanisms such as the conditions within the corrosion ring were either too acidic or alkaline for any precipitate to form but they also showed that within one corrosion ring the likely pH rise from oxygen reduction (for example) did not provide a good explanation for the ring structure. They also suggested that a convection process pushed corrosion product towards the boundary of the corrosion ring but this model has not been tested.[12] It is still not clear how corrosion rings formed and influenced corrosion halos in the work of Hughes et al., and similarly, how the corrosion halos in the current work developed. It can only be concluded that the RE(MAcet)₃ inhibitors were affecting corrosion halo formation.

Pr(MAcet)₃ also reduced the number of S-phase particles that showed evidence of trenching in the particle periphery, an example of which is site G in the secondary electron image for the Pr(MAcet)₃ sample (Figure 3c). Andreatta et al. suggested that on AA2024 clad with AA1050, in the presence of CeCl₃ not all particles were actively corroding at one time. As the CeCl₃ deposited and covered one particle, other particles would then become active which led to further deposition of Ce onto the alloy surface.[13] It is possible that the Pr(MAcet)₃ inhibitor was able to stifle the dealloying process on a number of S-phase particles, however, trenching still took place on other sites as they became active. A simpler explanation is the deposition of a thin film which covered the presence of localised trenching around the IM Particle which will be further discussed in section 4.2. The Ce(MAcet)₃ may have also limited the effects of trenching but it was not obvious from the results obtained in this work.

4.2. Inhibitor deposition of Ce(MAcet)₃ and Pr(MAcet)₃

The deposition of the RE metal was not always observed at the same location for AA2024-T3 surfaces immersed in the presence of either Ce(MAcet)₃ or Pr(MAcet)₃. It was previously proposed that after depositing on the surface of AA2024, progression of corrosion would cause local increases in alkalinity/acidity. A percentage of the deposited RE-organic molecules would hydrolyse and the released RE ion would be free to deposit as oxide/hydroxides at other sites on the alloy surface.[14-16] Similarly, it is likely that a percentage of the deposited RE(MAcet)₃ inhibitor molecules partially dissociated and deposited at varied sites on the AA2024-T3 surface. The RE metal would have deposited as oxides/hydroxides and limit the oxygen reduction reaction at cathodic sites while the MAcet⁻ molecule may also deposit at various sites which may not always be at the same location as the RE oxides/hydroxides. Furthermore, other species containing the RE metal, substrate oxides, such as Al, and the MAcet anion may also deposit on the surface resulting in a mixed and complex thin film.

The reduced visibility of the polish marks over the alloy matrix is a possible indication for the presence of an inhibitor film. Both Hughes et al.[17] and Campestrini et al.[18] suggested aluminium dissolution was necessary to allow for the deposition of cerium species on an AA2024 matrix. It should be noted that both authors were investigating the formation of cerium-based conversion coatings and the corresponding surfaces may have been significantly different to the as-polished surface in the current work. Dissolution of the matrix may have contributed to the reduced visibility of the polishing marks but the phenomenon is still not understood.

In summary, surface of the AA2024-T3 alloy exposed to these RE(MAcet)₃ inhibitors were likely to have a complex, heterogeneous combination of RE and aluminium oxide/hydroxides, deposited MAcet anion, and various species of the RE(MAcet)₃ molecule, depending on whether the interaction is with the matrix or the different IM particles. The observations in this work support the previously proposed mechanism of film formation, not only in the previous work on the RE(MAcet)₃ inhibitors, but other RE-organic inhibitor systems as well.[9, 14-16, 19] The mechanisms of surface interaction by Ce(MAcet)₃ and Pr(MAcet)₃ clearly have significant differences resulting in different surface film composition as well as inhibition efficiency. Further work is underway to better understand the exact mechanisms of film formation by these RE(MAcet)₃ inhibitors.

5. CONCLUSIONS

Both RE(MAcet)$_3$ inhibitors were found to reduce the current densities of the anodic arm of the polarisation experiments. The addition of Pr(MAcet)$_3$ significantly lowered cathodic current densities by up to two orders of magnitude as well as preventing trenching . The RE(MAcet)$_3$ inhibitors were found to limit the processes that produced corrosion halos around IM particles while depositing clusters of corrosion product over and around S-phase particles. The detection of RE metal and sulfur at different sites as well as the possibility of a thin film over the whole alloy surface all support previously proposed mechanisms of film formation and deposition by RE-organic inhibitors.

6. ACKNOWLEDGEMENTS

7. REFERENCES

1. Hughes AE, Glenn AM, Wilson N, Moffatt A, Morton AJ and Buchheit RG. A consistent description of intermetallic particle composition: An analysis of ten batches of AA2024-T3. (2013)
2. Boag A, Hughes AE, Glenn AM, Muster TH and McCulloch D. Corrosion of AA2024-T3 Part I. Localised corrosion of isolated IM particles. Corrosion Sci, 53(1) (2011)
3. Boag A, Hughes AE, Wilson NC, Torpy A, MacRae CM, Glenn AM, et al. How complex is the microstructure of AA2024-T3? Corrosion Sci, 51(8) (2009)
4. Buchheit RG, Grant RP, Hlava PF, McKenzie B and Zender GL. Local dissolution phenomena associated with S phase (Al2CuMg) particles in aluminum alloy 2024-T3. J Electrochem Soc, 144(8) (1997)
5. Hinton BRW, Arnott DR and Ryan NE. The inhibition of aluminium-alloy corrosion by cerous cations. Metals Forum, 7(4) (1984)
6. Twite RL and Bierwagen GP. Review of Alternatives to Chromate for Corrosion Protection of Aluminum Aerospace Alloys. Prog Org Coat, 33(2) (1998)
7. Buchheit RG, Hughes, A.E. Chromate and Chromate-Free Coatings. In: Moosbrugger C, editor. Corrosion: Fundamentals, Testing and Protection. Mterials Park, Oh, USA: ASM International; 2003. p. 720 -35.
8. Markley TA, Mardel JI, Hughes AE, Hinton BRW, Glenn AM and Forsyth M. Chromate replacement in coatings for corrosion protection of aerospace aluminium alloys. Materials and Corrosion, 61 (2010)
9. Ho D, Brack N, Scully J, Markley T, Forsyth M and Hinton B. Cerium dibutylphosphate as a corrosion inhibitor for AA2024-T3 aluminum alloys. J Electrochem Soc, 153(9) (2006)
10. Sastri VS, Green Corrosion Inhibitors: Theory and Practice, John Wiley & Sons (John Wiley & Sons), 2011.
11. Harvey TG, Hardin SG, Hughes AE, Muster TH, White PA, Markley TA, et al. The effect of inhibitor structure on the corrosion of AA2024 and AA7075. Corrosion Sci, 53(6) (2011)
12. Hughes AE, Boag A, Glenn AM, McCulloch D, Muster TH, Ryan C, et al. Corrosion of AA2024-T3 Part II Co-operative corrosion. Corrosion Sci, 53(1) (2011)
13. Andreatta F, Druart ME, Lanzutti A, Lekka M, Cossement D, Olivier MG, et al. Localized corrosion inhibition by cerium species on clad AA2024 aluminium alloy investigated by means of electrochemical micro-cell. Corrosion Sci, 65 (2012)
14. Forsyth M, Seter M, Hinton B, Deacon GB and Junk P. New 'Green' Corrosion Inhibitors Based on Rare Earth Compounds. Australian Journal of Chemistry, 64(6) (2011)
15. Hill J-A, Markley T, Forsyth M, Howlett PC and Hinton BRW. Corrosion inhibition of 7000 series aluminium alloys with cerium diphenyl phosphate. J Alloy Compd, 509(5) (2011)
16. Markley TA, Forsyth M and Hughes AE. Corrosion protection of AA2024-T3 using rare earth diphenyl phosphates. Electrochim Acta, 52(12) (2007)
17. Hughes AE, Gorman JD, Miller PR, Sexton BA, Paterson PJK and Taylor RJ. Development of cerium-based conversion coatings on 2024-T3 Al alloy after rare-earth desmutting. Surf Interface Anal, 36(4) (2004)
18. Campestrini P, Terryn H, Hovestad A and de Wit JHW. Formation of a cerium-based conversion coating on AA2024: relationship with the microstructure. Surf Coat Technol, 176(3) (2004)
19. Garcia SJ, Markley TA, Mol JMC and Hughes AE. Unravelling the corrosion inhibition mechanisms of bi-functional inhibitors by EIS and SEM–EDS. Corrosion Sci, 69 (2013)

8. AUTHOR DETAILS

R. Catubig graduated as a Materials Engineer from Monash University in Victoria, Australia. He is currently undertaking his PhD studies under the supervision of Maria Forsyth, Bruce Hinton, Anthony Hughes and Ivan Cole. His PhD project attempts to understand the mechanisms of inhibition by rare earth merpcatoacetate inhibitors on the aerospace alloy, AA2024-T3.

Professor M. Forsyth is the Associate Director of ARC Centre of Excellence for Electromaterials Science. Her research is directed towards development and understanding of charge transport at metal/electrolyte interfaces and within electrolyte materials. These include a wide range of ionic liquids, polymer electrolytes and plastic crystals. Using this understanding, her team collaborates very productively with colleagues within academia, CSIRO, DSTO as well as industry to design new materials and processes to control and optimise these phenomena in two key areas - corrosion and electrochemical devices.

Professor B. Hinton is a well-known figure in metal finishing, corrosion processes, inhibition and prevention. Though Bruce is currently retired, during his career as Principal Research Defence scientist he provided great contributions to several organisations in prevention of corrosion, specifically on aircraft structures. He continues to give advice and support to research and students alike to this day.

Dr I. Cole is a Chief Research Scientist at CSIRO and was previously the Deputy Chief of the CMSE division. His depth of expertise in material science and mathematical modelling allowed him to work in areas such as manufacturing and aerospace alloy corrosion protection. He was awarded the Silver Medal, BAE Systems Chairman's Award for Innovation and the Guy Benough Award throughout the course of his career. He remains at CSIRO, offering his skill and knowledge to colleagues and students.

Dr A. Hughes has been involved in multiple studies during the course of his career, such as surface science, metal finishing, alloy corrosion and corrosion inhibition. He has been awarded with the BAE SYSTEMS Chairman's Silver Award for Innovation as well as an award for Innovation from CSIRO. He remains at CSIRO lending his expertise not only to industrial partners but also to students and interns.